Measurement, Modelling and Simulation of Videoconference Traffic from VBR Video Encoders*

S. Kouremenos[1, 2, †], S. Domoxoudis[1, 2], V. Loumos[2] and A. Drigas[1]

skourem@mail.ntua.gr, sdomo@imm.demokritos.gr, loumos@cs.ntua.gr, dr@imm.demokritos.gr

1. National Center for Scientific Research ''DEMOKRITOS''
DTE/YE Applied Technologies Department, NetMedia Lab
P.O. Box 15310 Gr. Ag. Paraskevi, Attiki, Greece

2. National Technical University of Athens ''NTUA''
School of Electrical and Computer Engineering, Multimedia Technology Laboratory
P.O. Box 15780 Gr. Zographou, Attiki, Greece

Abstract

In this paper, we contribute measurement and modelling results on discrete-event queueing studies on the network performance of videoconference traffic encoded by variable bit rate video encoders over IP networks. The statistical analysis and modelling of extensive data compressed - during realistic talking heads communication - by the encoders of the videoconferencing tool ViC, namely, NV, NVDCT, H.261, H.263, H.263+, BVC and CellB (the traffic patterns of which, to the best knowledge of these authors, haven't been studied in their entirety) suggest that although the fit of the actual frame-size sequence histogram with a Gamma probability distribution function, using the method of moments, is not accurate, a careful choice of the autocorrelation parameter by calculating the autocorrelation decay *not* at the initial lags, but rather through taking the long-term trends into account, can lead to a conservative - with respect to queueing - and simple generalization of the short range dependent DAR and GBAR models. By comparing the buffer overflow estimation given by extensive simulation runs of the models against the one given by the actual videoconference data, all being included as the video source of a single-server queueing system implemented in ns-2 simulator, we confirm our claims and the importance of the long-term trends of the autocorrelation function on queuing performance.

***Key-words*:** videoconference traffic, network performance, VBR encoders, modelling, simulation, queueing, ViC, NV, NVDCT, H.261, H.263, H.263+, BVC, CellB, GBAR, DAR

Introduction

Videoconference traffic (especially H.26x encoded) is expected to account for large portions of the multimedia traffic in future heterogeneous networks (wire, wireless and satellite). The videoconference traffic models for these networks must cover a wide range of traffic types and characteristics because the type of the terminals will range from a single home or mobile user (low video bit rate) to a terminal connected to a backbone network (high video bit rate). Furthermore, successful videoconference traffic modelling can lead to a more economical network usage, leading to lower communication costs and a more affordable and of higher quality service to the end-users. However, the variation of the videoconference communication parameters (which in most cases are the target video bit rate, target frame rate and the used encoder), the differences in the video coding algorithm implementations and finally the variety of the visual contents (head and shoulders, sign

* This paper is an extended version of the paper presented at the second international working conference ''HET-NETs '04''(Ref. [28])

† Corresponding author: skourem@mail.ntua.gr, skourem@central.ntua.gr
Tel: 0030 6503143
Fax: 0030 7799784

language, movies, telemedicine) turn accurate videoconference traffic modeling into a complex procedure.

Partly due to the above reasons, videoconference traffic modelling and performance evaluation have been extensively studied in the literature and a wide range of modelling and simulation methods exist[‡]. Results of relevant early studies [2], [4], [5], [6], [7], [8], [10], concerning the statistical analysis of variable bit rate videoconference streams being multiplexed in ATM networks, indicate that the histogram of the videoconference frame-size sequence exhibits an asymmetric bell shape and that the autocorrelation function decays approximately exponentially to zero. An important body of knowledge, in videoconference traffic modelling, is the approach in [7] where the DAR(1) [1] model is proposed. More explicitly, in this study, the authors noted that AR models of at least order two are required for a satisfactory modelling of the examined H.261 encoded traffic patterns. However, in the same study, the authors observed that a simple DAR(1) model, based on a discrete-time, discrete state Markov Chain performs better - with respect to queueing - than a simple AR(2) model. In the same study, the parameters of the DAR(1) model were matched to the frame-size sequence histogram (fitted to a Gamma probability distribution function by the method of moments) and the exponential autocorrelation decay rate (derived from the AR(2) model). The results of this study are further verified by similar studies of videoconference traffic modelling [9] and vbr video performance and simulation ([8] and [13]). Moreover, a special software-assisted model, namely TES, [12] can simulate a video data trace producing a frame-size sequence that matches accurately the sample frame-size sequence histogram and autocorrelation function. The TES model, although it is accurate thanks to its ability to produce correlated pseudorandom uniformly distributed numbers, is too complex to be used in real time prediction or to be integrated in common simulators. Furthermore, in [10], the authors showed that the DAR(1) model has certain failings in modelling the performance of a single traffic source (i.e. a non-multiplexed environment). Instead, they proposed a generic Markov-renewal process model. However, in [16], D.P.Heyman claimed that a Markov renewal process has the disadvantage of not being parameterized by some simple summary statistics of the data trace. In the same study, the author noted that the DAR(1) model is not effective as a single source model because its sample paths have ‘‘flat spots’’ and do not ‘‘look like’’ the data trace. Instead, he proposed and evaluated the GBAR(1) process, as an accurate and well performed single-source videoconference traffic model. However, in the current study, we will show that the DAR model performs similarly with the GBAR model with respect to queueing (as a single source model) if a careful choice of the autocorrelation decay rate is employed.

The DAR(1) and GBAR(1) models provide a basis for videoconference traffic modelling through the matching of basic statistical features of the sample traffic. They are classical AR models, Short-Range[§] Dependent (SRD) and have the advantage of being easily implemented and integrated in simulator packages. On this basis and towards the modelling of videoconference traffic encoded by the ViC Intra-H261 encoder, the author in [19] proposed a DAR(8) model using the Weibull instead of the Gamma density for the fit of the sample histogram. Furthermore, in the same study, the author claimed the evidence of Long-Range Dependence (LRD) in the videoconference traces. However, in [20], the authors concluded that LRD has minimal impact on videoconference traffic modelling. In the same

[‡] It must be noted, here that the current study focuses on the study of the traffic generated by videoconference encoders and not by generic vbr video encoders like MPEG-2, MPEG-4. This being the case, studies of full-motion video traffic modelling, although highly contributing to the area of network performance analysis, are not examined.

[§] As referenced in [15] and later in [20], Long-Range Dependence (LRD) is not critical in videoconference traffic modelling.

study [20], the authors introduced a Continuous Markov chain model, called C-DAR(1), which is based on the DAR(1) model and is suitable for theoretical analysis. Looking at C-DAR(1) model as a Markov modulated rate process, as in [3], the same study's authors applied the fluid-flow method to compare the C-DAR(1) versus a trace-driven simulation. The C-DAR(1) model, as an analytically tractable model via the fluid-flow method, has the advantage of being ''steady''[**] in its prediction. This feature constitutes it directly applicable to theoretical studies of videoconference traffic modelling, but not to common discrete-event simulation modelling studies.

Relevant newer studies of videoconference traffic modelling reinforce the general conclusions obtained by the above earlier studies by evaluating and extending the existing models and also proposing new methods for successful and accurate modelling. In [21], H.263+ coded vbr video traffic in ATM networks was studied and the authors proposed a new model, called DAR(M), which is a compound DAR(1) model. The DAR(M) model analyses the number of cells in each type of a frame MacroBlock (MB) separately (I-coded, P-coded and N-coded). The final DAR(M) model is the mean of the DAR(1) models for each type of MB. In the same study, for the purpose of traffic modelling, the authors used the typical methods of DAR(1). In [22], a study of videoconference traffic (H.261 and H.263) measurement and simulation indicated the influence of the session parameters (codec, quality, frame rate) on the generated traffic pattern. Again, the sample histogram had a bell-shape and the autocorrelation function decayed quickly to zero. An extensive public available library of frame size traces of MPEG-4, H.263 and H.263+ encoded video was presented in [23] along with a detailed statistical analysis of the generated traces. In the same study, the use of movies, as visual content, led to frames generation with a Gamma-like frame-size sequence histogram (more complex when a target rate was imposed) and an autocorrelation function that quickly decayed to zero. A normal mixture distribution, as a method for fitting the sample histogram, was proposed in [24], and it was proved that it performed better than the simple Gamma and Log-normal distributions.

In [26], the authors observed that the DAR and GBAR models, although they are applicable to videoconference traffic modelling, they cannot model a variety of sources and perform unsteadily. To overcome this unsteadiness, the same authors adjusted the DAR model by introducing a marginal matching technique and a random variable chosen from a uniform distribution. Of particular relevance to our work is the approach in [25], where an extensive study on multipoint videoconference traffic (H.261-encoded) modelling techniques was presented. In this study, the authors discussed methods for correctly matching the parameters of the modelling components to the measured H.261-encoded data derived from realistic multipoint conferences (in ''continuous presence'' mode). Two new histogram-based methods for fitting the empirical frame-size histogram, namely, LVMAX and C-LVMAX were proposed. C-LVMAX was indicated as the one that can capture conservatively - with respect to queueing - the sample histogram due to its conservativeness near the tail. In the same study, it was highlighted that the autocorrelation decay rate should be not equal to the sample autocorrelation at lag-1, if the long-term trends in the autocorrelation decay are to be preserved. On this basis, the authors presented a new method for fitting the autocorrelation function (a method also adopted in the current study).

The above methods certainly constitute a valuable body of knowledge. However, these methods haven't been applied to the traffic generated by the entirety of the encoders used in the global videoconference market. ViC is a video conferencing tool which, although can be

[**] Here, using the term ''steady'' we refer to the advantage of the C-DAR model of being numerically treated and as a result providing a unique solution for each set of initial conditions. On the contrary, and as will be shown later, discrete-event models like DAR and GBAR need several independent replications to become steady-stated.

run for one-to-one conferences, is primarily intended as a multiparty conferencing application. It can be used in different computing environments and can accommodate both lower and higher bandwidth conditions. For the above reasons, ViC is widely used in web oriented systems for videoconferencing and collaborative work over IP networks (e.g. VRVS [www.vrvs.org]). Some of the encoders supported by ViC, like NV and Intra-H261, are widely used in palmtops and pocket PCs (e.g. Linux iPAQ [internet2.motlabs.com/ipaq/]) thanks to their effective performance and cheap processing needs.

Furthermore, most of the previous studies use movies as the video source of their experiments that exhibit abrupt scene changes. However, the traffic patterns generated by differential coding algorithms depend strongly on the variation of the visual information. For videoconference, visual information should not contain abrupt scene changes, as videoconference coding algorithms were designed for a typical head and shoulders content (with respect to talking heads communication).

In addressing the context just stated this study undertook measurements of the videoconference traffic encoded, during realistic head and shoulders experiments, by the ViC encoders. The basic contributions of our work can be summarized as follows: presentation of the encoded data statistical quantities, comparison of the encoders' traffic with respect to network performance, traffic modelling results, simulation proposal of the measured traffic and finally comparison and evaluation of the proposed modeling parameters. It is stressed that traffic modeling, in this paper, focuses on queueing studies on the network performance. Thus, particular attention is paid on properties such as the long-term trends in the autocorrelation function of the frame-size sequence and the tail behavior of the frame-size histogram.

The rest of the paper is structured as follows: section 1 describes the experiment characteristics and comments upon the statistical quantities of the measured data. Section 2 contributes modelling results with the DAR and GBAR models and discusses appropriate methods for modelling the encoded traffic. The simulation and evaluation results of section 3 confirm the claims of the previous sections and provide valuable conclusions for the implementation of the simulation models. Finally, section 4 culminates with conclusions and pointers to further research.

1. Description of the Experimental work

The study reported in this paper undertook measurements of the IP traffic generated by different vbr encoders, most of which have never been studied in literature. More explicitly, we measured the traffic generated by seven of the encoders included in the videoconference software tool ViC (version v2.8ucl1.1.6). These are[††]: NV [11], NVDCT [11], H.261 [29], H.263 [31], H.263+ [29], BVC [34] and CellB [30]. The JPEG [29] encoder was not examined as it produced large frames and a high video bit rate. This is attributed to the fact that in its coding algorithm, the entire frames are coded via the JPEG still image standard (the encoder does not utilize a block-based conditional replenishment algorithm). The PVH [14] encoder was not studied, too, as it utilizes a video compression algorithm that produces multiple layers in a progressively refinable format and tolerates packet loss. Finally, the RAW standard produces uncompressed data and as a result is out of interest in the current study.

Table 1 exhibits a brief comparison of the examined encoders. For the ViC encoders, compression is achieved by removing the spatial (intraframe) and the temporal (interframe) redundancy. In intraframe coding, a transform coding technique is applied at the image

[††] Although a newer encoder, namely, H.264, exists, ViC and most videoconference clients do not support it.

blocks, while in interframe coding, a temporal prediction is performed using motion compensation or another technique. Then, the difference or residual quantity is transform coded. At this point, we should note that the CellB encoder is quite different. While the other encoders search for blocks that have changed and compress them using transform coding (e.g. DCT or Haar), and the output is finally quantized and, usually, Huffman encoded, the CellB encoder is computationally symmetric in both encoding and decoding and it utilizes fixed colormap and vector quantization techniques in the YUV color space to achieve compression. Finally, CellB performs intraframe compression by representing 4-by-4 blocks of pixels using cell codes and interframe encoding using skip codes.

Concerning the measurement work, we used the methodology graphically represented in Figure 1: importing an offline created content (a person speaking with mild movement and no abrupt scene changes) through a digital video camera input (uncompressed RGB-24 format), we configured ViC to transmit the encoded data to a network sniffer (a pc running the program ‘‘Ethereal’’ [33]). The duration of each experiment was 1 hour and the settings of ViC were configured as follows: the video bit rate at 320 Kbps, video frame rate at 15 fps and the video window size at QCIF (parameters required for a high quality talking heads communication). For the purpose of comparing the different encoders’ traffic, the same content and settings were used in all the experiments. In each case, the UDP packets were captured by the traffic monitoring software and the collected data were further post-processed at the frame level[‡‡] by tracing a common packet timestamp. The produced frame-size sequences were used for further statistical analysis.

Some primary conclusions, as supported by the experiments’ results (see Table 2 and the column charts of Figure 2), arise concerning the statistical trends of each encoder traffic pattern. Initially, we observe that the encoders tend to reach the target video frame rate specified in the experimental settings (except H.263+). Moreover, NVDCT produces lower video bit rate than NV does. This is also observed at the H.26x series. Specifically, H.263+ produces lower video bit rate than H.263 and H.261 do (see Figure 2(a)). This was expected, since the earlier encoder versions have improved compression algorithms than the prior ones. Secondly, despite the fact that the H.261 (Intra-H.261) and NV encoders are both transform coders and are in fact quite similar, the former produces lower video bit rate because it uses a discrete cosine transform (DCT) instead of a Haar transform, it uses a linear quantizer instead of dead-zone only quantizer and it applies Huffman coding to the run-length encoded symbols. Finally, the BVC encoder produces higher video bit rate than the H.261 encoder, as it uses a Haar transform. On the contrary, it produces lower video bit rate than the NV encoder as it applies a Huffman coding to the run-length encoded symbols (for more information see [17], [29], [34]-[36]). It may also be observed that the mean video bit rate values achieved are in all cases much lower than the respective maximum specifications of the ViC settings, reflecting the fact that the visual content did not exhibit dramatic scene changes, frequent zooms or other such effects. This fact constitutes are results applicable to different experimental conditions, where the target video bit rate would be higher than the mean video bit rate exhibited by the encoders and a similar ‘‘head and shoulders’’ content would be used. This is also verified by the study in [25], where the statistical features of the traffic patterns remained invariant for the different scenarios of the target video bit rate. That means that the accomplishment of other experiments with different parameters is of no point as the encoded traffic would be reasonably captured by a common model.

Furthermore, the tendency of the encoders to reach the target mean frame rate (except H.263+), led to similar results (to those of the mean video bit rate values) for the mean and

[‡‡] It is important to note, here, that analysis at the MacroBlock (MB) [21] level has been examined and found to provide only a typical smoothing in the sample data. We believe that the analysis at the frame level is simpler and offers a realistic view of the traffic.

maximum frame size values of the encoders' traffic patterns, see Figures 2(b) and 2(d). The same feature is noted at the variance values (see Figure 2(c)), with the exception of H.263 whose variance value is smaller than that of H.263+. Of particular interest in Figures 2(b), (c), is that the frame-size sequences of the H.263+, CellB and BVC encoders have almost equal variance values and that the correspondent sequences of the CellB and BVC encoders have almost equal mean frame sizes values.

The above results, as presented in Table 2 and compared through the column charts of Figure 2, besides constituting a valuable data set for performance analysis studies, are modelling results directly applicable to full simulation models. As will be discussed shortly, the mean frame size and the variance of the frame-size sequence are input parameters for calculating the shape and scale parameters of the Gamma density. Furthermore, the minimum and maximum frame sizes can be used to assign the values for the min and peak video bit rate, required for the construction of the Markov chain states of the DAR model. Finally, these comparative results, based on the same content encoding, can simplify the analytical studies by providing a measure of the difference of the modelling parameter values. For instance, if the mean frame size and the variance value of an encoder video traffic (e.g. H.261) were calculated by an offline measurement, then the correspondent values of the other encoders could be relatively estimated[§§].

2. Traffic Analysis

The analysis of the measured traffic confirms the general body of knowledge that literature has formed concerning videoconference traffic. In brief, the frame-size sequence can be represented as a stationary stochastic process, with a frequency histogram of an approximately Gamma Probability Distribution Function (PDF) form and an AutoCorrelation Function (ACF) that quickly decays to zero (see Figures 3(a),(d),(g),(j),(m),(p),(s) and 4(a)-(g)). In checking for stationarity, each frame sequence corresponding to an encoder was split in ten windows and then the empirical density function for the frame size was calculated from the sample, in each window. These windows were found to be very much alike, property suggesting that the sequence is stationary. This is in accordance with previous studies (e.g. [7], [25]) where stationarity was found to apply for H.261-encoded traffic.

Examining more thoroughly the sample histograms, we note that the smoothed frame-size frequency histograms of the NV, NVDCT, H.261 and BVC encoders have an almost similar asymmetrical bell-shape with a tail[***] towards the large frame sizes (see Figures 3(a),(d),(g),(s) while a more symmetrical shape appears in the H.263 histogram (Figure 3(j)). An obvious similarity in the H.263+ frame-size sequence is the reason of its narrow bell-shaped histogram (Figure 3(m)) (the small H.263+ variance value denoting the same too). Finally, the CellB histogram appears to be discrete (Figure 3(p)), feature that can be attributed to the discrete compression methods utilized by the CellB encoder.

Concerning the characteristics of the sample ACFs, we remark a similar behavior for all the encoders (see Figures 4(a)-(g)) with notable stronger correlations in the H.26x series (even stronger for the H.263+ encoder, see Figure 4(e)). These strong ACF correlations (implying periodicities in the traffic pattern) are attributed to the size similarities (temporal redundancy) that exist between sequential video frames. This phenomenon, though, does not influence the ACF long-term decay rate, that is a critical parameter in queueing.

[§§] In fact, this can not be assured for the entirety of the encoders in the market, but mainly for the ViC encoders.

[***] Tail behavior is critical in queueing and will be examined thoroughly during analysis.

The above results constitute the short-range dependent DAR(1) and GBAR(1) models directly applicable to full modelling and analytic treatment of the traffic. These models are described analytically in the section to follow.

2.1. The DAR(1) and GBAR(1) models

The DAR(1) [1, 7] model produces a frame-size sequence according to the transitions of a discrete time Markov Chain, of the form:

$$P = \rho I + (1-\rho)Q \tag{1}$$

where ρ is the autocorrelation parameter at lag-1, I is the identity matrix and Q is a rank-one stochastic matrix with all rows equal to the probabilities resulting from the negative binomial density of the form:

$$y = f(x/r,P) = \binom{r+x-1}{x} P^x (1-P)^x, \quad x = 0,1,... \quad r > 0, \quad 0 < P < 1 \tag{2}$$

Instead of directly dealing with the discrete density (2), in the following we work with its continuous counterpart, namely the Gamma density - used to fit the sample histogram - of the form:

$$y = f(x/p,\mu) = \frac{1}{\mu^p \Gamma(p)} x^{p-1} e^{-x/\mu}, \quad \mu, p > 0, \quad x \geq 0, \quad \Gamma(p) = \int_0^\infty u^{p-1} e^{-u} du \tag{3}$$

Although several methods concerning the calculation of the Gamma density parameters exist, the authors in [7] and [16] proposed the method of MOMents (MOM). According to this method, when the mean, m, and the variance, v, of the data sample are known, the p and μ parameters of the Gamma density (3) are estimated by the following equations:

$$p = \frac{m^2}{v} \tag{4}$$

$$\mu = \frac{v}{m} \tag{5}$$

Correspondingly, the parameters r and P of the negative binomial density (2) can be calculated from the sample mean and variance by the following equation:

$$r = \frac{m^2}{v-m} \tag{6}$$

$$P = \frac{m}{v} \tag{7}$$

or by the parameters of the correspondent Gamma density with p and μ parameters as follows:

$$r = \frac{p\mu}{\mu - 1} \tag{8}$$

$$P = \frac{1}{\mu} \tag{9}$$

A frame-size sequence generated with the DAR(1) model has an exponentially decaying autocorrelation function equal to ρ^k and a marginal frame-size density with probability masses equal to the elements of the common rows in Q.

In the GBAR(1) [16] model, the simulated source trace is generated by a stationary stochastic process:

$$X_n = A_n X_{n-1} + B_n, \quad n=0,1,2,... \tag{10}$$

where X_n is the n_{th} generated frame size, A_n ($A_n(\alpha,\beta)$)is a random number chosen from the Beta probability distribution of the form:

$$y=f(x/a,b)=\frac{1}{B(a,b)} x^{a-1}(1-x)^{b-1}, \quad a,b>0, \quad 0<x<1 \tag{11}$$

where: $B(a,b)=\int_0^1 t^{a-1}(1-t)^{b-1}dt$ and B_n ($B_n(b,\mu)$)is a random number chosen from the Gamma density (3) with a different shape parameter. The frame-size sequence autocorrelation generated from (10) is equal to ρ^k. The parameters of the Beta and Gamma densities in (10) are calculated using the MOM method as follows: if p and μ are the parameters derived from (4) and (5) - same as the ones used for the DAR model - and ρ is the measured ACF decay rate then the parameters α and b of the Beta density $B_n(a,b)$ (11) are calculated as follows (for a value of ρ near 1):

$$a = \rho p \tag{12}$$

$$b = (1-\rho)p \tag{13}$$

The parameters b and μ of the Gamma density $B_n(b,\mu)$ for GBAR are calculated from (13) and (5), correspondingly. The non-integer frame-size values generated from (10) are rounded to the nearest integer. Although, this rounding process could be avoided by using the negative binomial density (2) instead of the gamma density (3), the gamma density is more practical and its usage does not influence the statistical quantities of the generated video source (as indicated in [16], too).

2.2. Matching of the Modelling Parameters

Now, we may turn to the discussion of the methods used for matching the parameters of the modelling components to the data and for combining these components into the analytical DAR and GBAR models. According to section 2.1, it is obvious, that the modelling parameters required for the implementation of the DAR and GBAR models are the p and μ parameters of the Gamma density and the autocorrelation decay rate ρ. The paragraphs to follow are devoted to the calculation of these parameters.

For the purpose of fitting the Gamma density to the sample frame-size sequence histogram, although various full histogram-based methods have been tried in literature, (see for example [24], [25]), we encourage the use of the MOM method as it requires only the sample mean frame size and variance values. Thus, taking into account that the sequence is stationary - and as a result the mean and the variance values are almost the same for all the sample windows - it is evident that only a part of the sequence is needed to calculate the Gamma density parameters. Furthermore, this method has the feature of capturing accurately the sample mean video bit rate (feature derived from the fact that the method uses the mean frame size to calculate the Gamma density parameters). The numerical values of the p and μ parameters for all the encoders, calculated by the equations (4) and (5), with the correspondent inputs of Table 2, appear in Table 3.

To evaluate the MOM method, with respect to its accuracy in fitting and its conservativeness in queueing, besides plotting the sample histogram versus the MOM

density (see Figures 3(a),(d),(g),(j),(m),(p),(s)), we applied the following method: we plotted the sample quantiles from the sample cumulative frequency histogram and the model quantiles from the incomplete Gamma density: $f_{inc}(x,p)=\frac{1}{\Gamma(p)}\int_0^x e^{-t}t^{p-1}dt$ where $\Gamma(p)$ derives from (3) and p, μ from (4) and (5) correspondingly. The Q-Q plot of this method refers to cumulative distributions (probabilities of not exceeding a threshold). Thus, the tail behavior for the fit is indicated by the neighborhood of the quantiles around 1. If the model's quantiles are lower than the sample quantiles in that neighborhood, the model is considered to be conservative with respect to queueing, see Figures 3(b),(e),(h),(k),(n),(q),(t). For more detail around that neighborhood, the complementary sample frequency histogram is plotted together with the complementary Gamma density $(1-f_{inc}(x/\mu,p))$ in the large frames region (see Figures 3(c),(f),(i),(l),(o),(r),(u)). The final plot gives valuable indications about the tail behavior of the model (tendency of the model to move to high bandwidth states) and a measure of its conservativeness concerning queueing.

The conclusions derived from the above method are as follows: in most cases, the MOM method did not manage to follow closely the histogram in all quantiles (especially in the first ones and more notable in the case of H.263+ (Figure 3(n)). However, this phenomenon is not critical with respect to queueing as what is important is the conservativeness of the model at the higher rate states (large frame sizes). Moreover, the complementary density plots indicate that in most cases the model is tail-conservative (see Figures 3(c),(f),(i),(r),(u)). This phenomenon, though, is less intense in the case of H.263 and H.263+ (Figures 3(i),(o)). Despite the certain drawbacks of the MOM method, we encourage its usage as it has the advantage of being tail-dominant and not requiring full histogram information. Finally, as will be commented upon later, this inaccuracy of the MOM method is negligible if a careful choice of the autocorrelation decay rate is performed.

At this point, we may discuss about the calculation of the autocorrelation decay rate ρ. From the Figures 4(a)-(g), it is observed that the ACF graphs exhibit a reduced decay rate beyond the initial lags. This is a behaviour also noted in earlier studies [6], [25]. To fit the sample ACF, we applied the model proposed in [25], namely, Compound Exponential Fit (CEF). This model fits the autocorrelation function with a function equal to a weighted sum of two geometric terms:

$$\rho_\kappa = w\lambda_1^\kappa + (1-w)\lambda_2^\kappa, \text{ with } |\lambda_2| < |\lambda_1| < 1 \quad (14)$$

where $\lambda_{1,2}$ are the decay rates. In the above equation, the value of the autocorrelation parameter λ_1 is very critical as it tends to capture the long-term behavior of the autocorrelation function. What is notable is that using this model, the autocorrelation parameter ρ is chosen *not* at lag-1, as in DAR(1) and GBAR(1) models.

This method was tested with a least squares fit to the autocorrelation samples for the first 500, 1000 and 5000 lags for each encoder (for each modelling case we name the model's fit as CEF(500), CEF(1000) and CEF(5000) and the calculated parameter ρ_{500}, ρ_{1000} and ρ_{5000} correspondingly)[†††]. For each encoder, the λ_1 parameter numerical values appear in Table 3, while the fitted model graphs are compared to the sample ACFs in Figures 4(a)-(g). From the CEF model fits, it is obvious that the property of capturing the ACF long-term trends is reflected more intensely by the CEF(5000) fits, where the decay rate has a value higher than 0.999 (approximately 1). However, the decay rate values for videoconference traffic mostly

[†††] At this point, we have to notice that modelling at further than 5000 lags is of no point as the autocorrelation values for these lags are easily captured by the CEF(5000) model.

appeared in literature were found to be near 0.985 in [7] or higher, near 0.995, in [25]. Given the above modelling results, the following question naturally arises: what is the proper value of the decay rate ρ towards a successful implementation of the DAR and GBAR models? Is this parameter critical in queueing results?

In the section to follow, towards reliable answers to the above question, the discussed modelling components are combined into complete traffic models with the DAR and GBAR methods. Furthermore, the different modelling parameters are evaluated and validated comparing sample-based against model-based discrete-event simulations in a single-server queueing system implemented in the ns-2 simulator.

3. Simulation and Evaluation of the Modelling Components

For the purpose of evaluating the modelling methods discussed in the previous section, we followed the approach that is graphically represented in Figure 5. According to this approach, a traffic source (sample-based or model-based) is included in a single-server queueing system implemented in ns-2 (system to be described analytically later). In this case, modelling evaluation derives from the comparison of the queue buffer overflow estimation given by discrete-event simulation [18] using the actual frame-size sequence against the queue buffer overflow estimation given by the simulated (with DAR or GBAR) frame-size sequences[‡‡‡]. Using the same process, we compared and validated the different ACF decay rate values (ρ_{500}, ρ_{1000} and ρ_{5000} correspondingly). Before proceeding to the results of the above approach, we devote the following paragraphs in describing the exact steps followed to generate the model-based sequences with the DAR and GBAR models.

In implementing the DAR model, the values of the r and P parameters of the negative binomial density and the decay rate ρ (in each case of 500, 1000 and 5000 lags) are required. The r and P parameter values, as calculated by the equations (6) and (7), are presented in Table 3. Moreover, the DAR model (1) demands the representation of the frame-size sequence with a constant number of states, whose probabilities values will fill the rows of the stochastic matrix Q. After extensive frames generations with the DAR model, we concluded that a 30-state markov chain can simulate satisfactorily the actual data and capture accurately the sample mean rate. These states can be easily chosen by dividing the interval between the maximum and the minimum frame size of the sequence into 30 frame-size states. So, if x_{min} is the minimum and x_{max} the maximum frame-size value then a reasonable state step s is $s = (x_{\max} - x_{\min})/30$, with s rounded to the nearest integer. The rate of each state can be easily calculated by the relative mean rate of a histogram window, as follows: if P_i is the probability mass of frame size S_i (derived from the negative binomial density) then the rate value of the state is equal to $\sum_{i=1}^{s} p_i s_i * f / \sum_{i=1}^{s} p_i$ rounded to the nearest integer where f is the frame rate of the trace (derived from Table 2) and $\sum_{i=1}^{s} p_i$ is the probability mass of the certain state (that will fill the correspondent element of the matrix Q in (1)).

Concerning the GBAR model, we calculated the Beta density parameters α and b from the equations (12) and (13) and the b and μ Gamma density parameters from (13) and (5) (for each value of the ρ parameter). The values of these parameters, presented in Table 3, can be directly fed as input to the GBAR process (10).

[‡‡‡] We would like to note, here, that although the DAR and GBAR models could be implemented directly in ns-2, all simulations in our study are offline implemented using the Matlab Statistical ToolBox [37]. That means that in fact, all simulations held in ns-2 are discrete-event trace-driven simulations (see [27] for more information on trace-driven simulation).

Applying the above, we conducted 250 simulation runs (independent replications) for each encoder and each modelling case. The number of the generated frames was chosen equal to the actual frame-size sequence length. By the analysis of the generated sequences, we noted that in each group of generated sequences (same encoder and same value of ρ), the sequences statistical trends were found to be different. This phenomenon is attributed to the fact that DAR and GBAR are stochastic processes and consequently their result is uncertain. In this case, we average the statistical quantities of each group to find mean performances of different models. For each group, we calculated the standard deviations of the mean video bit rate (see Table 4 for analytical results). With reference to this table, some first conclusions arise concerning the modelling methods applied: firstly, it is observed that the GBAR model exhibits a closer bound to the actual mean video bit rate and variance than the DAR model. Moreover, in most cases, we note that when the value of ρ increases (regularly from ρ_{500} to ρ_{5000}), the achieved mean video bit rate increases, too. This phenomenon confirms our initial claim and the claim in [25] that the conservativeness of a model depends strongly on its ability to capture the ACF long-term trend. Even then, though, the standard deviation value is quite large so that mean rate values lower than the actual one could be exhibited. Moreover, the existence of opposite phenomenon (where the video bit rate value decreases while ρ increases, as in the implementation of GBAR for CellB) leads us to the conclusion that the current results are inadequate for the extraction of a general rule. However, some obvious conclusions are the following: in general, the GBAR model appears to be steadier than the DAR model and, at this point, seems to be better solution for simulating videoconference traffic (it is more complex than DAR, though). Especially, in the case of the H.263+ encoder, the DAR model provides results, far too conservative, while the GBAR model manages to captures accurately the mean video bit rate of the actual traffic. Perhaps, a more careful choice of the ACF decay rate of the H.263+ traffic sequence could lead to better results for the DAR model. However, as will be commented upon later, a modulation of the generated data to the sample rate can overcome the inaccuracy of the models.

We believe that the most critical point in queueing studies is the steadiness of the mean video bit rate of the simulated trace. However, the general conclusion, as supported by the results of Table 4, is that the DAR and GBAR models perform unsteadily due to their stochastic nature. Even in cases of close bound to the sample mean rate, a value of standard deviation higher than 4Kbits/sec can lead to a deviation from the actual mean video bit rate. This deviation, although it is small, would lead to inaccurate results in a queueing system. A positive deviation, though, would lead to conservative results. However, this cannot be assured. This fact constitutes reliable the following comparison of the sample versus the generated traces in a queueing system with a common server capacity.

Having described our simulation approach, we may describe the single-sever queueing system implemented in ns-2 that was used as an evaluation and comparison testbed. In ns-2, an output queue of a node is implemented as a part of each link whose input is that node. The definition of the link then includes the way to handle overflow at that queue. More explicitly, we used the following simple topology (see Figure 7): consider a simple network composed of only two nodes *S* (Source) and *D* (Destination), and one link connecting them. We run on node *S* the sample or simulated videoconference traffic of mean video bit rate *C* Kbits/sec. The destination of the traffic is node *D*. The video frame inter-arrival time is selected constantly equal to *1/f* (where *f* is the actual sample frame rate from Table 1). The link connecting the two nodes has a speed of *1.1*C* Kbits/sec (server capacity *10*% higher than the client capacity), a propagation delay of *0* ms and a buffer at its input of infinite size (so that no actual overflow occurs).

Deploying the above queueing system in ns-2 [32], we conducted simulations (the duration of the simulation being 1 hour) with each of the available sample and generated

traces. In each case, we assured to monitor the queue buffer length size every *0.1*sec. Given that no overflow occurs, it is evident that the complementary probability distribution of the monitored buffer length frame-size sequence - monitored at each clock time - gives buffer overflow probabilities for a selected queue buffer size. The comparison of the complementary density given by the sample frame-size sequence and the one given by the simulated data is directly applied for further validation and evaluation of the modelling components. For each modelling case (combination of model and decay rate value) the complementary buffer size densities of the simulated data (derived from the mean buffer-size sequence of the independent replications) and the correspondent sample are plotted together (see Figures 8-14 for each encoder correspondingly). In each figure caption, we note the modelling parameters (encoder, model, decay rate used e.g. (NV, DAR, $\rho = \rho_{500}$)). The probabilities values are always assigned at the logarithmic scale.

The basic conclusions, as derived from our evaluation results, graphically represented in Figures 7, are the following: The autocorrelation decay rate value influences strongly the densities slope for both models, DAR and GBAR. In fact, the densities slope increases proportionally to the decay rate value. This feature confirms our claim hat the ACF long-term trend is very critical in queueing analysis. That means, that the model's conservativeness (in this case, the tendency of the model to estimate higher overflow probabilities for a given buffer length size than the sample) is relatively proportional to the ACF decay rate value. Furthermore, for all the encoders, except H.263+, decay rate values higher than 0.995 are required to constitute the model steadily conservative. This fact is notable in all simulation cases when the decay rate ρ is calculated at the first 500 lags - see Figures 8(a),(d)-14(a),(d) - where the DAR and GBAR densities plots are not always higher than the sample densities. On the contrary, it is concluded by Figures 8(b),(e)-14(b),(e), where ρ is calculated at the first 1000 lags, that a decay rate value between 0.998 and 0.999 (except H.263) can lead to steadily conservative models in most cases. For the third case, where ρ is higher than 0.999 - see Figures 8(c),(f)-14(c),(f) - although the models appear to be more conservative, they fail to fit the sample densities at the small buffer sizes (for logarithmic probability values between -0.3 and 0.0). This phenomenon, being less notable when ρ is equal to ρ_{1000}, can be attributed to the MOM's inaccuracy at the first quantiles. In overall, the DAR and GBAR models perform similarly, with the DAR model being more conservative in most cases. Finally, for H.263+, a decay rate value between 0.98 and 0.99 seems to be enough for conservative modelling (see Figure 12).

4. Conclusions

The current study is a contribution of modelling and simulation results for a variety of existing videoconference encoders for talking heads communication. An extensive analysis of the measured data, a careful but simple modelling of the frame-size sequences and the extensive evaluation of the modelling components, led us to the general conclusion that the most critical point in modelling videoconference traffic is the long-term trend of the frame-size sequence autocorrelation function and not the exact fit of the frame-size histogram. In all experimental and modelling cases, we noticed that although the moments fit was not accurate, a choice of the autocorrelation parameter higher than 0.99 could lead to accurate simulation results- with respect to queueing - and simple generalization of the DAR and GBAR models. Moreover, the DAR model was found to perform similarly with the GBAR process. This fact combined with the indicative simplicity and faster implementation of the DAR model in comparison with the GBAR (almost 2min slower in one replication) consist it as the proper videoconference (single-source) simulation model for queueing studies.

Finally, the Tables 2, 3 and 4 constitute a valuable data set for performance evaluation and queueing studies on videoconferencing applications.

Future work includes the validation of our modelling approach with different videoconference contents (low motion and high motion) and the implementation of the C-DAR model as a further numerical validation process.

Acknowledgements

The authors would like to thank Dr K. Kontovasilis for valuable discussions, suggestions and encouragement.

References

[1] P.A. Jacosb and P.A.W.Lewis, Time series generated by mixtures, J. Time Series Analysis (1983), vol. 4, no. 1, pp. 19-36.

[2] B. Maglaris, D. Anastassiou, P. Sen, G. Karlsson and J. D. Robbins, Performance models of statistical multiplexing in packet video communications, IEEE Trans. Commun. (1988), 36(7): 834–843.

[3] D. Mitra, Stochastic theory of a fluid model of producers and consumers coupled by a buffer, Adv. Appl. Prob. (1988), vol. 20, p. 646-676.

[4] R. Kishimoto, Y. Ogata, and F. Inumaru, Generation interval distribution characteristics of packetized variable rate video coding data streams in an ATM network, IEEE JSAC (1989), 7(5):833–841.

[5] H. S. Chin, J. W. Goodge, R. Griffiths and D. J. Parish, Statistics of video signals for viewphone-type pictures, IEEE JSAC (1989), 7(5):826–832.

[6] M. Nomura, T. Fujii and N. Ohta, Basic characteristics of variable rate video coding in ATM environment, IEEE JSAC (1989), 7(5):752–760.

[7] D. P. Heyman, A. Tabatabai and T. V. Lakshman, Statistical analysis and simulation study of video teleconference traffic in ATM networks, IEEE Trans. Circuits Syst. Video Technol. (1992), 2(1):49–59.

[8] D. M. Cohen and D. P. Heyman, Performance modelling of video teleconferencing in ATM networks, IEEE Trans. Circuits Syst. Video Technol. (1993), 3(6):408–422.

[9] D.P. Heyman, T.V. Lakshman, Modeling Teleconference Traffic from VBR Video Coders, IEEE ICC (1994), pp.1744-1748.

[10] D.M. Lucantoni, M.F. Neuts, Methods for Performance Evaluation of VBR Video Traffic Models, IEEE/ACM Transactions on Networking (1994), Vol.2, No.2, pp. 176-180.

[11] R. Frederick, Experiences with real-time software video compression, Xerox Parc (1994).

[12] B. Melamed, D. Raychaudhuri, B. Sengupta and J. Zdepski, TES-Based Video Source Modeling For Performance Evaluation of Integrated Networks, IEEE Transactions on Communications (1994), Vol. 42, No. 10, 2773-2777.

[13] A. Elwalid, D. Heyman, T. V. Lakshman, D. Mitra, and A. Weiss, Fundamental bounds and approximations for ATM multiplexers with applications to video teleconferencing, IEEE JSAC (1995), 13(6):1004-1016.

[14] S. R. McCanne, Scalable Compression and Transmission of Internet Multicast Video, Report No. UCB/CSD-96-928, Computer Science Division (EECS) (1996), University of California, Berkeley, California 94720.

[15] A. Erramilli, O. Narayan, and W. Willinger, Experimental queueing analysis with long-range dependent packet traffic, IEEE/ACM Trans. Networking (1996), 4(2):209-223.

[16] D. P. Heyman, The GBAR source model for VBR videoconferences, IEEE/ACM Trans. Networking (1997), 5: 554-560.

[17] L. D. McMahan, Video Conferencing over an ATM Network, Thesis (1997), California State University, Northridge.

[18] M. Law and W. D. Kelton, Simulation Modeling and Analysis - 3nd Edition (1999), McGraw-Hill Higher Education.

[19] B. Ryu, Modeling and Simulation of Broadband Satellite Networks: Part II-Traffic Modeling, IEEE Communications Magazine (1999).

[20] S. Xu, Z. Huang, and Y. Yao, An analytically tractable model for video conference traffic, IEEE Trans. Circuits Syst. Video Technol. (2000), 10(1):63–67.

[21] G. Sisodia, L. Guan, M. Hedley, S. De, A New Modeling Approach of H.263+ VBR Coded Video Sources in ATM Networks, RealTimeImg(6) (2000), No. 5, pp. 347-357.

[22] K. Dolzer, W. Payer, On aggregation strategies for multimedia traffic, Proceedings of the 1st Polish-German Teletraffic Symposium (2000), Dresden.

[23] F. Fitzek and M. Reisslein, MPEG-4 and H.263 video traces for network performance evaluation, IEEE Network (2001), vol. 15, no. 6, pp. 40-54, Video traces available at http://www.eas.asu.edu/mre.

[24] W.C. Poon and K.T. Lo, A refined version of M/G/∞ processes for modeling VBR video traffic, Computer Communications (2001), vol.24, no.11, pp.1105-1114.

[25] C. Skianis, K. Kontovasilis, A. Drigas and M. Moatsos, Measurement and Statistical Analysis of Asymmetric Multipoint Videoconference Traffic in IP Networks, Telecommunications Systems (2003), Volume 23, Issue 1. pp. 95-122.

[26] L. Yan-ling, W. Peng, W. Wei-ling, A Steady Source Model for VBR Video Conferences, International Conference on Information Technology: Computers and Communications (2003), Las Vegas, Nevada, p. 268.

[27] F. Fitzek, P. Seeling, M. Reisslein, Using Network Simulators with Video Traces (2003), http://kom.aau.dk/~ff/documents/tracesim.pdf

[28] S. Domoxoudis, S. Kouremenos, V. Loumos and A. Drigas, Measurement, Modelling and Simulation of Videoconference Traffic from VBR Video Encoders, Second International Working Conference, HET-NETs '04, Performance Modelling and Evaluation of Heterogeneous Networks (2004), Ilkley, West Yorkshire, U.K., 26 - 28 July.

[29] Open Mash (http://www.openmash.org/)

[30] Sun Product Documentation, Sun Microsystems (http://docs.sun.com/db/doc/).

[31] H.263 Standard, Overview and TMS320C6x Implementation, White Paper, www.ubvideo.com.

[32] The Network Simulator - ns-2, http://www.isi.edu/nsnam/ns/

[33] Ethereal, The world's most popular network protocol analyzer, http://www.ethereal.com

[34] UCL Networked Multimedia Research Group, http://www.mice.cs.ucl.ac.uk/multimedia/

[35] IETF Request For Comments (RFC) Page, http://www.ietf.org/rfc.html

[36] Greek Universities Network – Mbone Multicast (http://www.teiath.gr/mbone/)

[37] The Matlab Statistics ToolBox 5 (http://www.mathworks.com/products/statistics/)

Table 1. A brief comparison of the examined encoders[§§§]

Encoder	NV	NVDCT	H.261	H.263	H.263+	CellB	BVC
Intraframe Coding	Haar	DCT	DCT	DCT	DCT	Cell Codes	Haar
Interframe Coding	Haar	DCT	-	DCT	DCT	Skip Codes	Haar

Table 2. Statistical quantities of the sample frame-size sequences

Encoder	NV	NVDCT	H.261	H.263	H.263+	CellB	BVC
Experiment Duration (sec)	3600						
# of Frames	50113	53336	53937	53453	17921	53749	53855
Mean Video Bit Rate (Kbits/Sec)	182	121	63	54	13	93	92
Mean Frame Rate	14	15	15	15	5	15	15
Mean Frame Size (Bytes)	1638	1023	527	457	331	779	766
Variance ($bytes^2$)	1589100	678870	174130	24588	401060	407130	467460
Min Frame Size (bytes)	24	24	78	196	80	77	40
Max Frame Size (bytes)	10284	6468	2718	2122	5343	5959	4658

Table 3. Values of the modelling parameters for the different ACF decay rate values

	NV	NVDCT	H.261	H.263	H.263+	CellB	BVC
	Gamma Density Parameters (using MOM)						
p	1.68902	1.54127	1.59437	8.50609	0.27242	1.49142	1.25564
μ	969.96887	663.67191	330.47803	53.76463	1,213.33648	522.47651	610.15460
	Autocorrelation Decay Rate ρ (using CEF)						
	at the first 500 lags						
ρ_{500}	0.9941	0.9941	0.9970	0.9946	0.9968	0.9934	0.9956
	at the first 1000 lags						
ρ_{1000}	0.9984	0.9981	0.9987	0.9959	0.9991	0.9983	0.9985
	at the first 5000 lags						
ρ_{5000}	0.9996	0.9997	0.9997	0.9995	0.9992	0.9997	0.9997
	Negative Binomial Density parameters for the DAR model						
r	1.69076639	1.54359945	1.59920646	8.66729693	0.27264964	1.49427861	1.25769994
P	0.00103096	0.00150677	0.00302592	0.01859959	0.00082417	0.00191396	0.00163893
	BETA Density parameters for the GBAR model						
	$\rho = \rho_{500}$						
α	1.67905804	1.53218009	1.58958428	8.46015588	0.27155317	1.48157526	1.25011385
b	0.00996524	0.00909351	0.0047831	0.04593288	0.00087176	0.00984336	0.00552481
	$\rho = \rho_{1000}$						
α	1.68632084	1.53834518	1.59229471	8.4712138	0.22611269	1.48888321	1.2537552
b	0.00270244	0.00292842	0.00207268	0.03487496	0.04631224	0.00253541	0.00188346
	$\rho = \rho_{5000}$						
α	1.68834767	1.54081122	1.59388908	8.50183572	0.27217974	1.4909712	1.25526196
b	0.00067561	0.00046238	0.00047831	0.00425304	0.00024518	0.00044743	0.00037669

[§§§] The presented information was retrieved from the source code of the ViC client found at the UCL Networked Multimedia Research Group's web site (http://www-mice.cs.ucl.ac.uk/multimedia/)

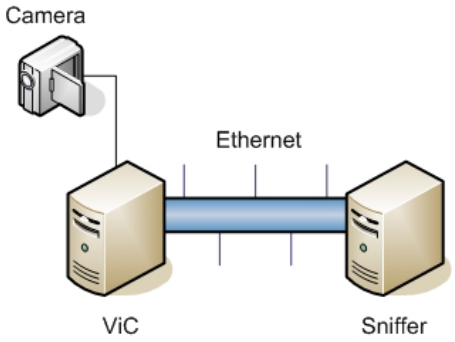

Figure 1. The experimental network topology

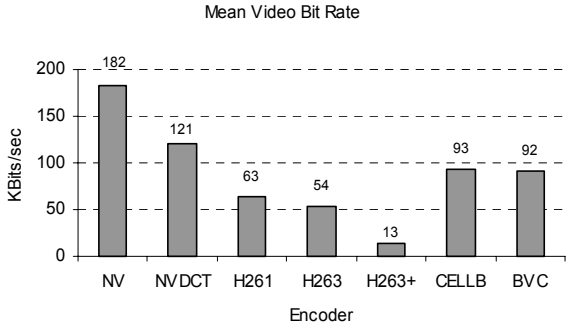

Fig. 2(a)

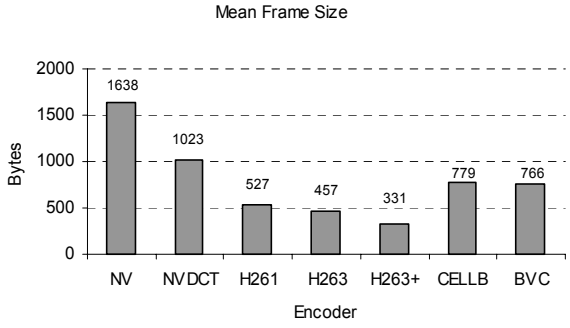

Fig. 2(b)

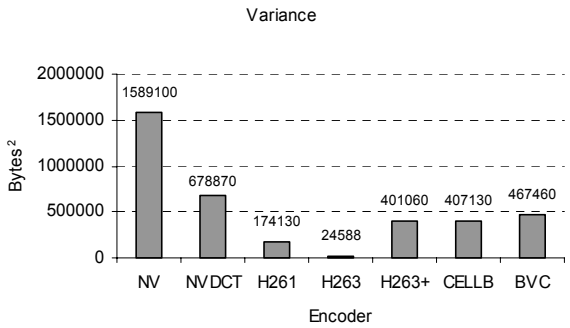

Fig. 2(c)

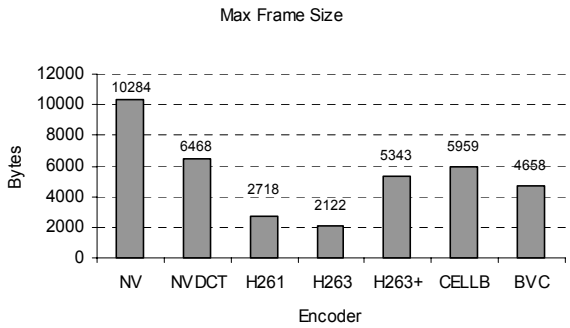

Fig. 2(d)

Figure 2. Column charts of the encoders' Mean Video Bit Rate (a), Mean Frame Size (b), Variance (c) and Maximum Frame Size (d)

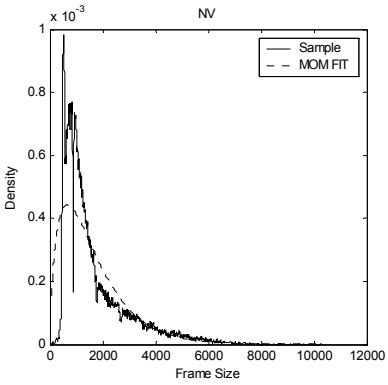

Fig. 3(a)

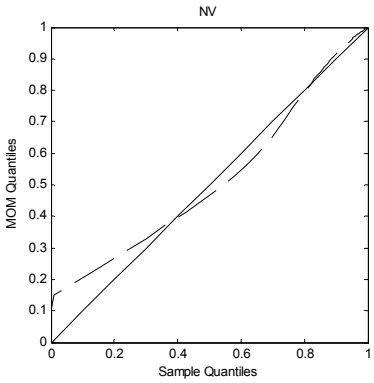

Fig. 3(b)

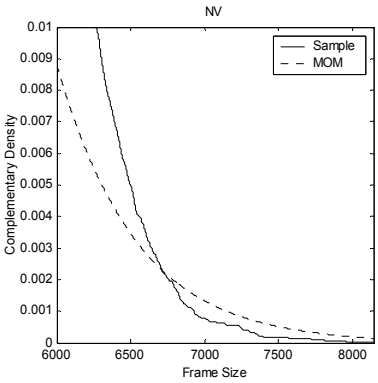

Fig. 3(c)

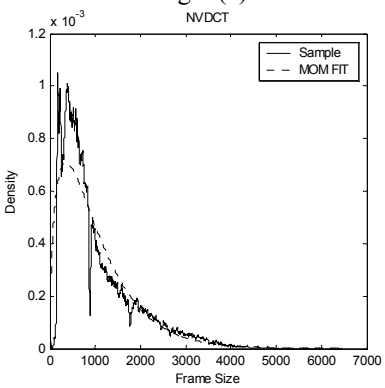

Fig. 3(d)

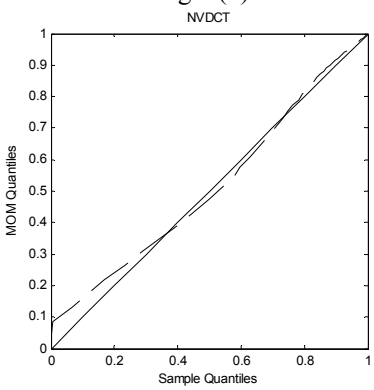

Fig. 3(e)

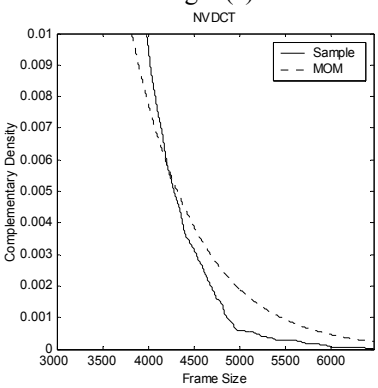

Fig. 3(f)

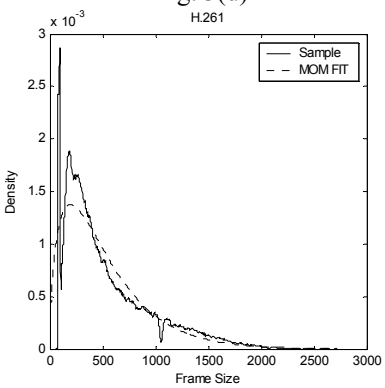

Fig. 3(g)

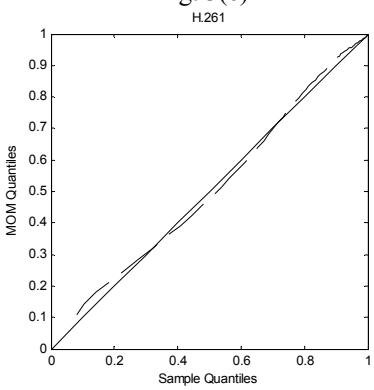

Fig. 3(h)

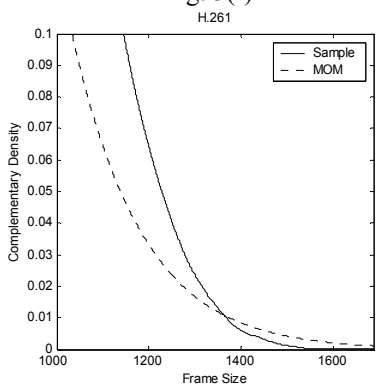

Fig. 3(i)

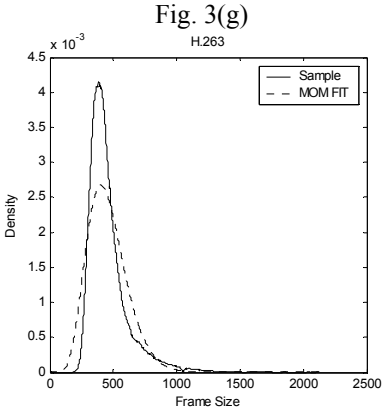

Fig. 3(j)

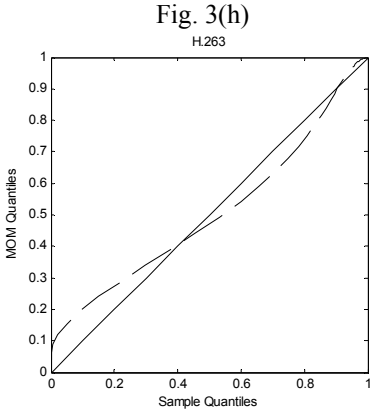

Fig. 3(k)

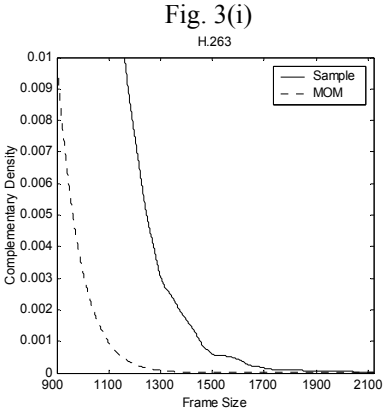

Fig. 3(l)

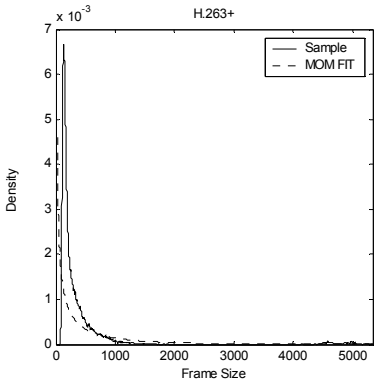

Fig. 3(m)

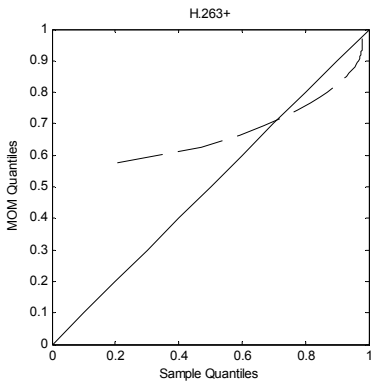

Fig. 3(n)

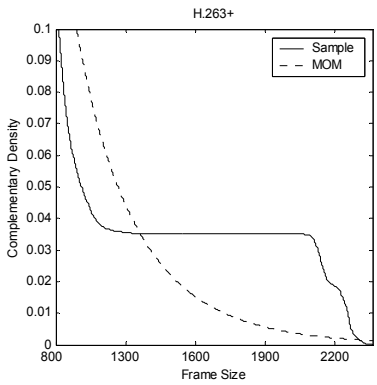

Fig. 3(o)

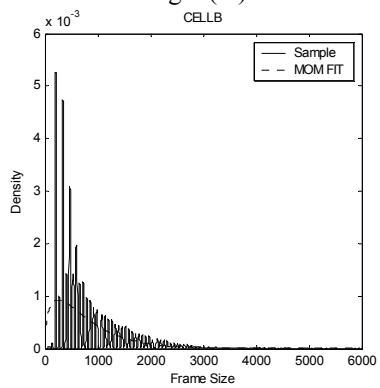

Fig. 3(p)

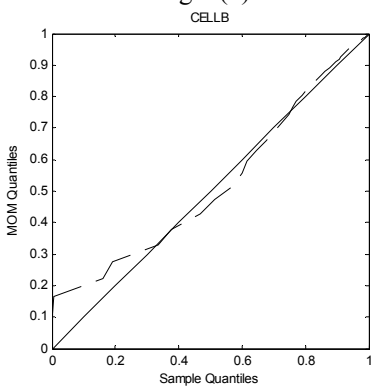

Fig. 3(q)

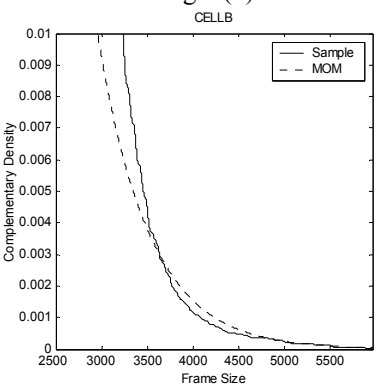

Fig. 3(r)

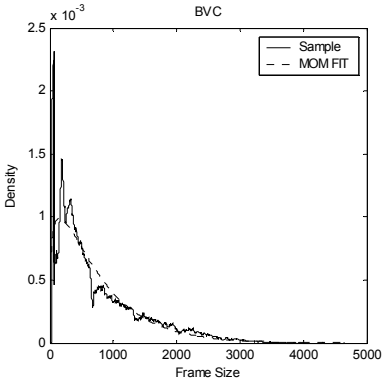

Fig. 3(s)

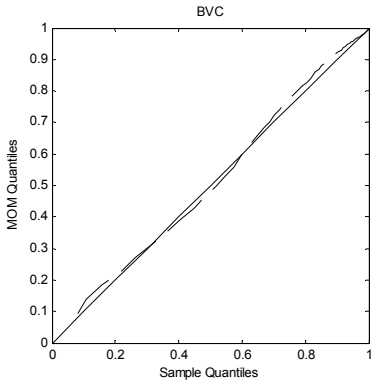

Fig. 3(t)

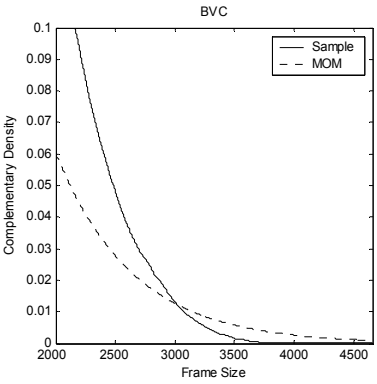

Fig. 3(u)

Figure 3. Frame-size histograms vs moment fit (a), (d), (g), (j), (m), (p), (s)
Q-Q Plots of histograms vs moment fit (b), (e), (h), (k), (n), (q), (t)
Complementary densities of frame-size histogram vs moment fit (c), (f), (i), (l), (o), (r), (u)

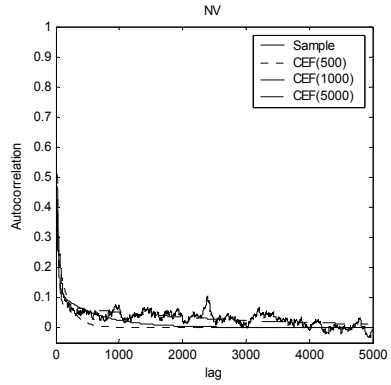

Fig. 4(a)

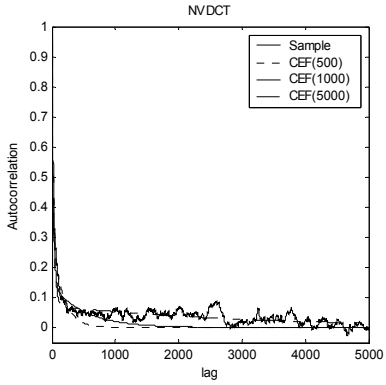

Fig. 4(b)

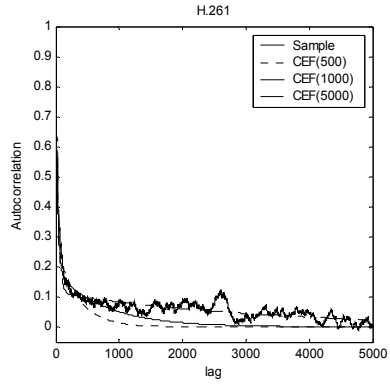

Fig. 4(c)

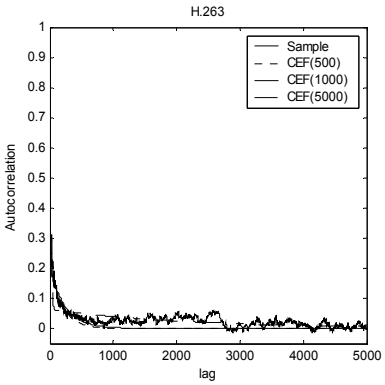

Fig. 4(d)

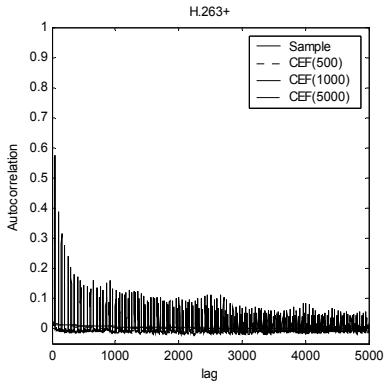

Fig. 4(e)

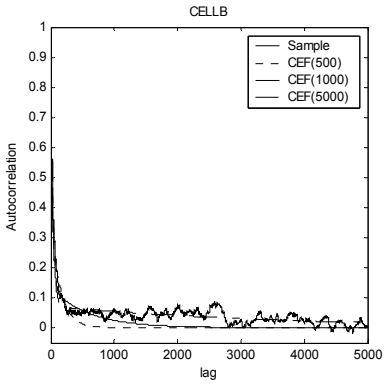

Fig. 4(f)

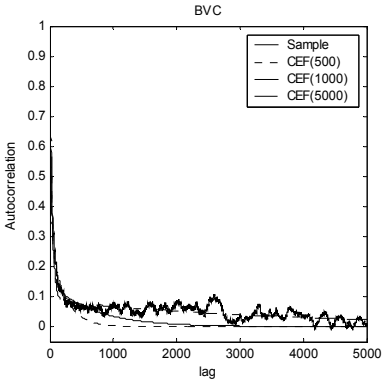

Fig. 4(g)

Figure 4. Autocorrelation Graphs and fitted CEF models at 500, 1000 and 5000 lags for each encoder (a) - (g)

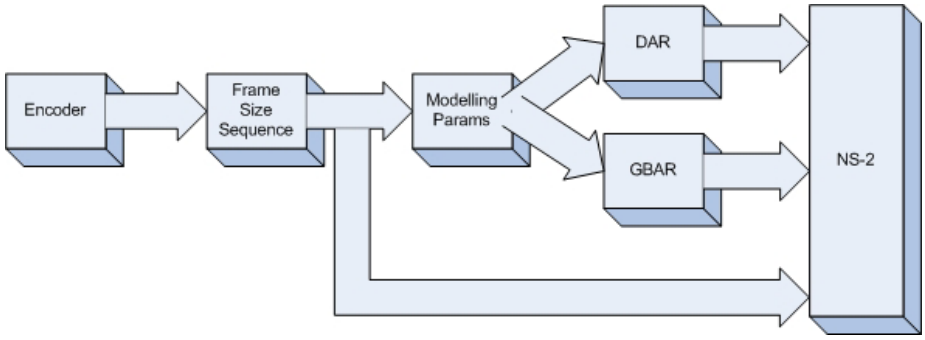

Figure 5. Overview of the modelling vs actual trace comparison approach

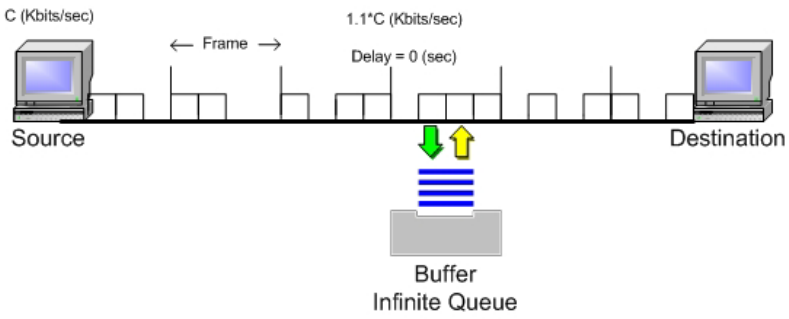

Figure 6. The single-server queuing system implemented in ns-2

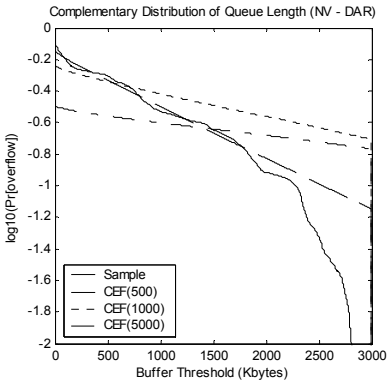

Fig. 7(a)

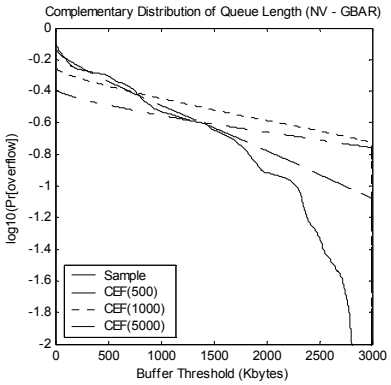

Fig. 7(b)

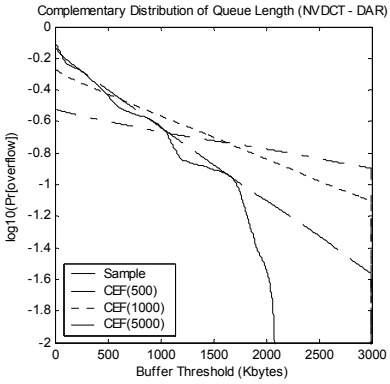

Fig. 7(d)

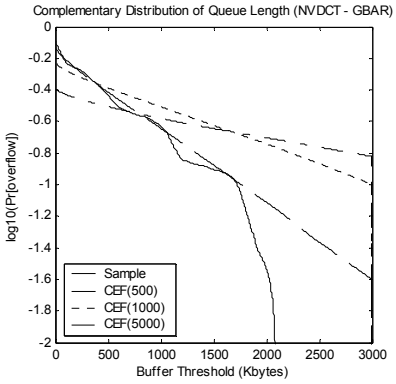

Fig. 7(e)

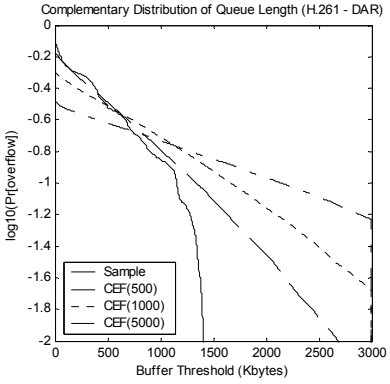

Fig. 7(g)

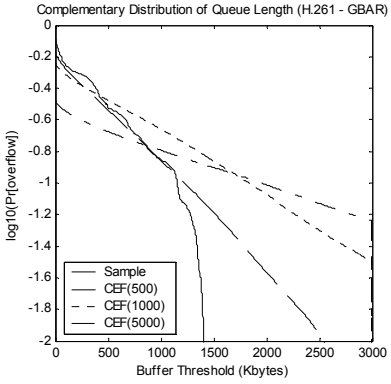

Fig. 7(h)

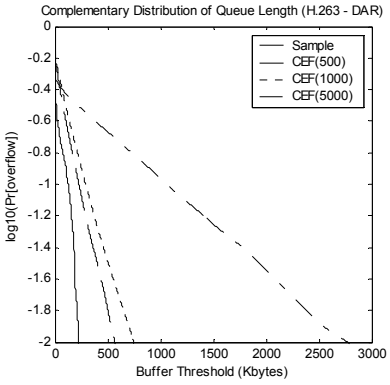

Fig. 7(i)

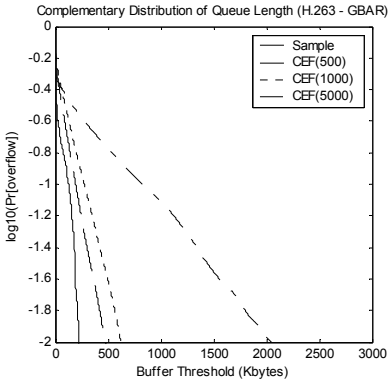

Fig. 7(j)

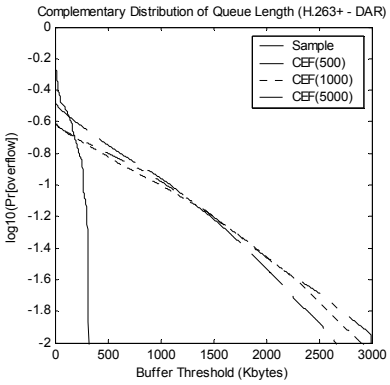

Fig. 7(k)

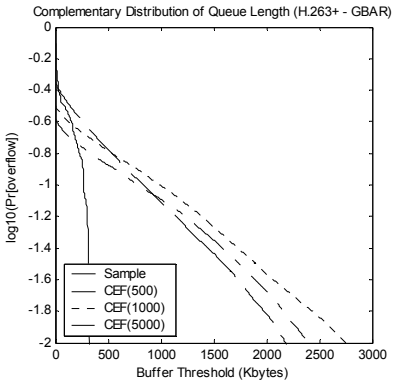

Fig. 7(l)

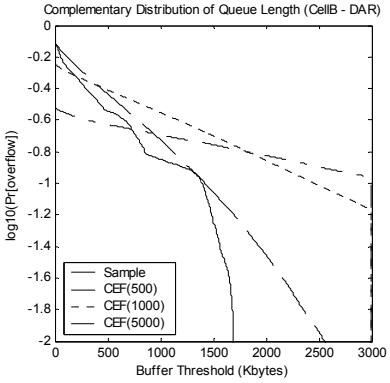

Fig. 7(m)

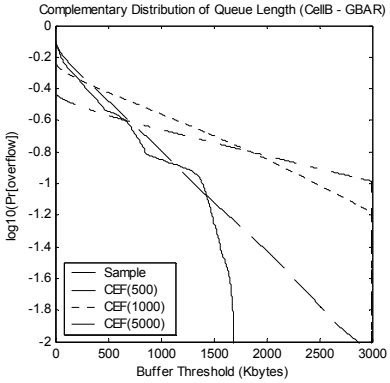

Fig. 7(n)

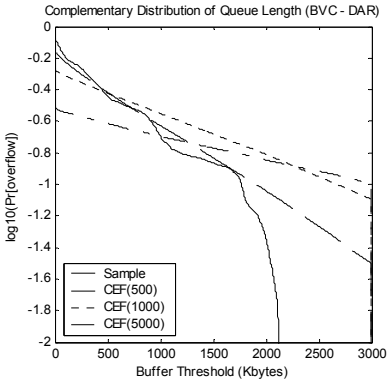

Fig. 7(o)

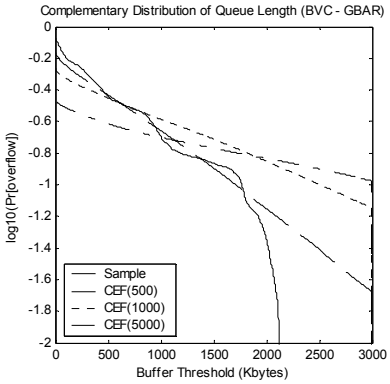

Fig. 7(p)

Figure 7. Complementary buffer overflow density plots of model vs sample simulation